JOURNAL OF SOLID STATE CHEMISTRY 81, 1–8 (1989)

Microdomains in the $CaFe_xMn_{1-x}O_{3-y}$ Ferrites. III. $0.5 \leq x \leq 0.9$

J. M. GONZÁLEZ-CALBET, M. VALLET-REGÍ, AND J. ALONSO

Departamento de Química Inorgánica, Facultad de Químicas, Universidad Complutense, 28040 Madrid, Spain

J. RODRÍGUEZ-CARVAJAL[1]

Instituto de Ciencia de Materiales de Barcelona (CSIC), Martí i Franqués s/n, 08028 Barcelona, Spain

AND J. FONTCUBERTA

Departament de Física Fonamental, Universitat de Barcelona, Diagonal 647, 08028 Barcelona, Spain

Received August 8, 1988; in revised form January 30, 1989

The study by electron diffraction and high-resolution electron microscopy of several samples of the $Ca Fe_xMn_{1-x}O_{3-y}$ system ($0.5 \leq x \leq 0.9$), prepared at high temperatures in air, shows that compositional variations can be achieved in several ways as a function of the x and y values: intergrowing microdomains, disordered intergrowths, and randomly dispersed oxygen deficiency accommodate the nonstoichiometry in these materials. © 1989 Academic Press, Inc.

Introduction

In a series of previous papers (*1–4*), we dealt with nonstoichiometry in the system $CaFe_xMn_{1-x}O_{3-y}$ in order to study the accommodation of the oxygen vacancies in AMO_{3-y} perovskites when the M positions are occupied by two cations able to adopt various oxidation states and several polyhedral environments.

Two series of samples of the title system were prepared at 1100 and 1400°C in air, respectively. An electron diffraction and microscopy study of the low-temperature (LT) samples (*1*) have shown that this system contains two solid solutions of the perovskite-type (P) (*5*) and of the brownmillerite-type (B) (*6*) and also an intermediate phase (G) with $A_3M_3O_8$ composition (*7, 8*) which makes disordered intergrowth with the B-type solid solution. High-temperature samples (HT) did accommodate the nonstoichiometry in a more complex manner showing a microdomain texture in the $0.2 \leq x \leq 0.4$ range (*2, 3*). Thus, the $x = 0.2$ sample was formed by three-dimensional twinned domains with the perovskite-type structure (PTD), while the $x = 0.4$ material was constituted by six sets of domains: three PTD and another three

[1] Present address: Institut Laue-Langevin, 156 X, 38042 Grenoble Cedex, France.

0022-4596/89 $3.00

sets of domains characterized by a brownmillerite-type structure (BTD).

In this paper, we report a study by electron diffraction and microscopy of the $CaFe_xMn_{1-x}O_{3-y}$ system, prepared at high temperature, in the region $0.5 \leq x \leq 0.9$.

Experimental

Samples of $CaFe_xMn_{1-x}O_{3-y}$ ($0.5 \leq x \leq 0.9$) were prepared from stoichiometric amounts of $CaCO_3$, α-Fe_2O_3, and $MnCO_3$ by heating at 1000°C in air for 48 hr to decompose the carbonates. Then, the mixtures were thoroughly reground, pelletized, and fired at 1400°C in air for 46 hr. Macroscopically homogeneous black powders were obtained after quenching to room temperature and characterized by X-ray powder diffraction, using silicon as internal standard.

Total amounts of calcium, iron, and manganese were confirmed by atomic absorption spectrometry. The amount of Mn^{4+} was determined, as proposed by Fyfe (*9, 10*) by dissolving the sample in hydrochloric acid and adding potassium iodide solution in the presence of acetylacetone. The iodine liberated was determined by titration with $Na_2S_2O_3$ solution in the presence of starch.

TABLE I

CHEMICAL ANALYSIS DATA OF THE HT SAMPLES AND UNIT CELL PARAMETER REFERRED TO THE PSEUDOCUBIC SUBCELL

x	Chemical composition	a_c (Å)
0.5	$CaFe^{3+}_{0.5}Mn^{4+}_{0.37}Mn^{3+}_{0.13}O_{2.685}$	3.775(1)
0.6	$CaFe^{3+}_{0.6}Mn^{4+}_{0.25}Mn^{3+}_{0.15}O_{2.625}$	3.784(1)
0.7	$CaFe^{3+}_{0.7}Mn^{4+}_{0.17}Mn^{3+}_{0.13}O_{2.585}$	G + B[a]
0.8	$CaFe^{3+}_{0.8}Mn^{4+}_{0.11}Mn^{3+}_{0.09}O_{2.555}$	G + B[a]
0.9	$CaFe^{3+}_{0.9}Mn^{4+}_{0.05}Mn^{3+}_{0.05}O_{2.525}$	3.822(1)

[a] G and B refer to the $A_3M_3O_8$ and brownmillerite cells, whose unit cell parameters are G(1), a = 5.476(1); b = 11.151(3); c = 5.360(1) Å; B(6), a = 5.5980(5); b = 14.7687(17); c = 5.4253(5) Å.

The oxidation state of iron was determined by chemical analysis with 0.1 N $K_2Cr_2O_7$ solution after dilution in HCl with an excess of Mohr's salt, confirming that all iron was in the III state of oxidation. Chemical compositions are listed in Table I.

Electron diffraction and microscopy were carried out on a Siemens Elmiskop 102 microscope equipped with a ±45° goniometer stage, kindly lent to us by the CSIC (Instituto de Ciencia de Materiales, sede D), Madrid, Spain. Specimens were ultrasonically dispersed in n-butanol and then mounted on carbon-coated microgrids.

Results and Discussion

The powder X-ray diffraction pattern of the $x = 0.5$ sample could be assigned to solid showing an average cubic perovskite-like structure with unit cell parameter a = 3.775(1) Å, although a slight broadening of Bragg reflections was observed. A similar situation was detected for the $x = 0.6$ material, where the increasing of the unit cell parameter (a = 3.784(1) Å) can be attributed to the smaller ionic size of Mn^{4+} with respect to both Fe^{3+} and Mn^{3+} (*11*).

Since the anionic vacancy concentration of both solids is very high ($y = 0.315$ and $y = 0.375$ for $x = 0.5$ and $x = 0.6$, respectively), a study by electron diffraction and microscopy is necessary in order to elucidate the microstructure of such materials.

Figure 1a shows the electron diffraction pattern of the $x = 0.5$ sample along the $[001]_c$ zone axis, indexed on the basis of the cubic perovskite subcell (subindex c refers to such a subcell). This pattern and those observed by tilting around both $\mathbf{a}_c^*$ and $\mathbf{b}_c^*$ axes reflects the same situation as that observed on the $x = 0.4$ material which was interpreted (cf. Ref. (*2*)) in terms of the intergrowth of six sets of microdomains: three of them having the perovskite-type structure (PTD) and the other three show-

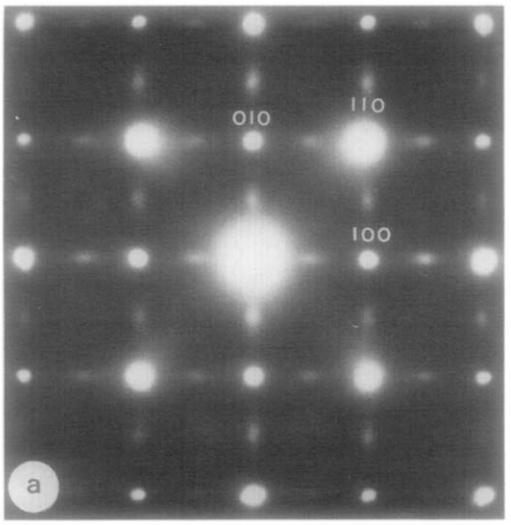

FIG. 1a. Electron diffraction pattern of the $x = 0.5$ sample along the $[001]_c$ zone axis.

ing the brownmillerite structure (BTD) with their long axis alternating at random in the three space directions. Certainly, the corresponding electron micrograph (Fig. 1b) shows the presence of microdomains where the amount of BTD seems to be slightly more abundant than that previously observed on the $x = 0.4$ sample (*2*, *3*).

The situation becomes different by increasing the amount of iron, since two types of crystals are observed when $x = 0.6$. Most of the crystals show the electron diffraction pattern appearing in Fig. 2a. The presence of two fourfold superlattices along $\mathbf{a}_c^*$ and $\mathbf{b}_c^*$ axes and extra spots located at $(\frac{1}{2}\ \frac{1}{2}\ 0)_c$ and equivalent positions suggest again a microdomain texture as already found in the previous sample which is reflected in the corresponding micrograph (Fig. 2b), where the following d-spacing can be recognized:

—Fringes at 14.8 Å in areas marked *Y* and *Z* corresponding to the d_{010}-spacing of a B-type cell oriented in two perpendicular directions.

—Other regions (*X* and *V*) in which the $\approx 5.5 \times 5.5$ Å fringes can be due either to the d_{001}- and d_{100}-spacing of a B-type cell or

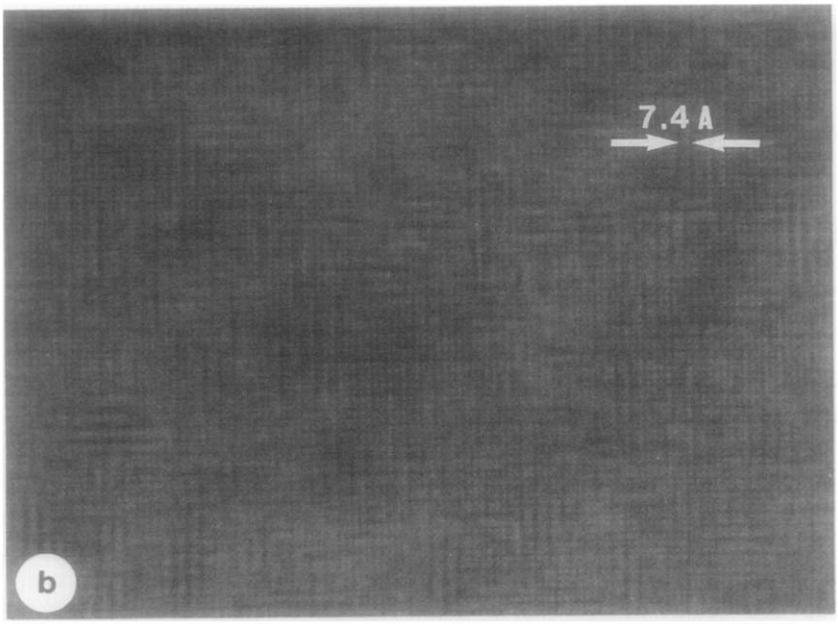

FIG. 1b. Corresponding electron micrograph.

the same spacing of an $\mathbf{a}_c\sqrt{2} \times 2\mathbf{a}_c \times \mathbf{a}_c\sqrt{2}$ P-type cell.

—Finally, fringes at 3.7 Å (in *T*) corresponding to the d_{020}-spacing of the P-type cell.

It must be noticed that reflections $(hk0)_B$, with $h + k = 2n + 1$, are forbidden in the *Pcmn* space group of $Ca_2Fe_2O_5$ (*6*). The appearance of such reflections in the diffraction pattern (Fig. 2a) may be due to slight modifications of the B structure when growing as microdomains or, more probably, to multiple scattering.

In order to complete the study of the reciprocal lattice, a series of tilts were performed around $\mathbf{a}_c^*$ and $\mathbf{b}_c^*$ axes. Figure 3a shows the electron diffraction pattern corresponding to the $[10\bar{2}]_c$ zone axis. The spots located at $(\frac{1}{2}\ \frac{1}{2}\ \frac{1}{4})_c$ and $(\frac{3}{2}\ \frac{1}{2}\ \frac{3}{4})_c$ indicate that the third perovskite axis also shows a fourfold superlattice. On the other hand, the diffraction maxima at $(1\ \frac{1}{2}\ \frac{1}{2})_c$ and equivalent positions correspond to the third perovskite-like domain, as schematically shown in Fig. 3b.

According to these results, we can conclude that these kinds of crystals are also constituted by the juxtaposition of three PTD and three BTD, the brownmillerite being for this composition the major component.

On the other hand, a few crystals of the $x = 0.6$ sample did show a different behavior. Figure 4 shows the corresponding electron diffraction pattern along the $[001]_c$ zone axis. Two threefold superlattices along $\mathbf{a}_c^*$ and $\mathbf{b}_c^*$ axes can be appreciated. Tilts around both axes give patterns indicating that the third pervoskite axis also shows a threefold superlattice. This is the way in which compositional variations are accommodated in $Ca_2LaFe_3O_{8.325}$, i.e., $Ca_{2/3}La_{1/3}FeO_{2.745}$ (*12, 13*), where the material was constituted by a microdomain texture whose reciprocal lattice was formed by the intergrowth of three reciprocal nets with

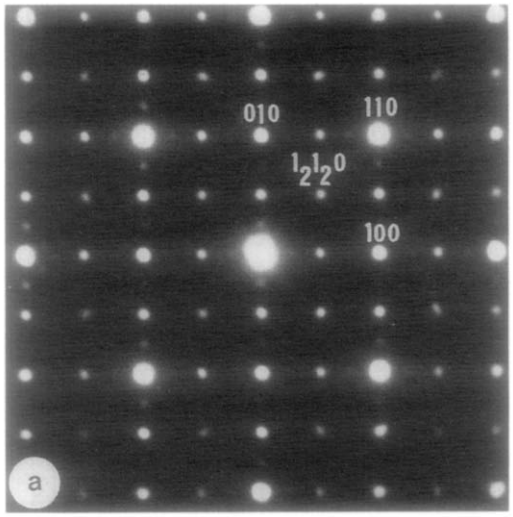

FIG. 2a. Electron diffraction pattern of the first type of crystals found in the $x = 0.6$ material. Zone axis $[001]_c$.

$\mathbf{a}_c\sqrt{2} \times 3\mathbf{a}_c \times \mathbf{a}_c\sqrt{2}$, the long axis alternating at random in the three space directions. It is worth emphasizing that such parameters are characteristic of an $A_2M_3O_8$, i.e., $AMO_{2.667}$ composition, where two octahedral layers alternate in an ordered way with a tetrahedral layer (*14*), the microdomain formation being accompanied by an oxidation process, i.e., of a decreasing in the vacancy concentration. However, in our $x = 0.6$ material, since the average anionic vacancy concentration is higher ($y = 0.375$) and the cationic ratio 2:1 is not established, most of the crystals accommodate the nonstoichiometry by formation of big domains of the brownmillerite-type structure.

For richer compositions in iron ($x \geq 0.7$), the X-ray diffraction patterns become similar to those observed in the low-temperature samples (*1*). When $x = 0.7$ and $x = 0.8$, most of the diffraction maxima can be assigned to a brownmillerite-type structure. However, there are some few peaks corresponding to the G-type structure. Electron

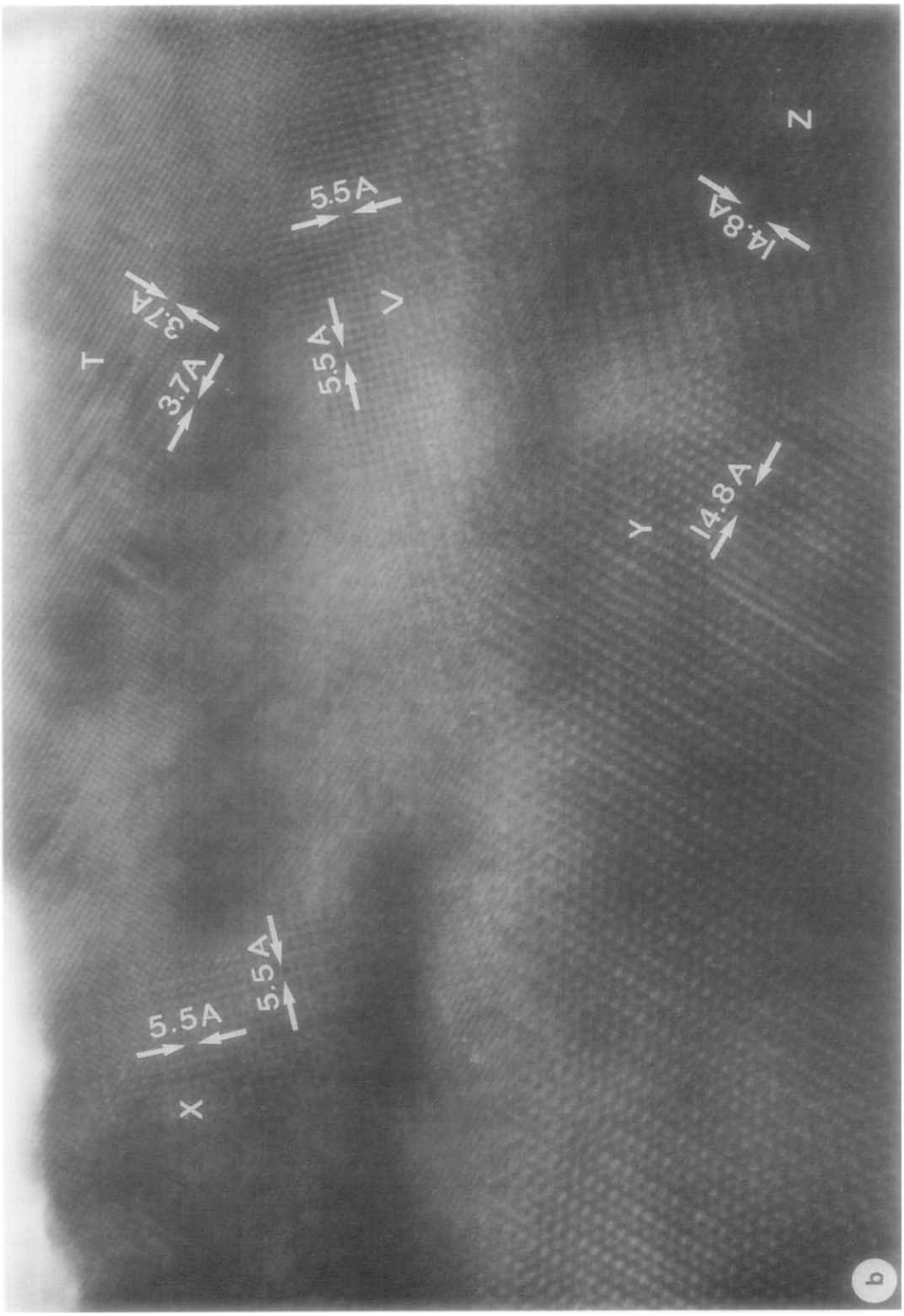

FIG. 2b. Corresponding electron micrograph showing big areas of BTD intergrowth with PTD.

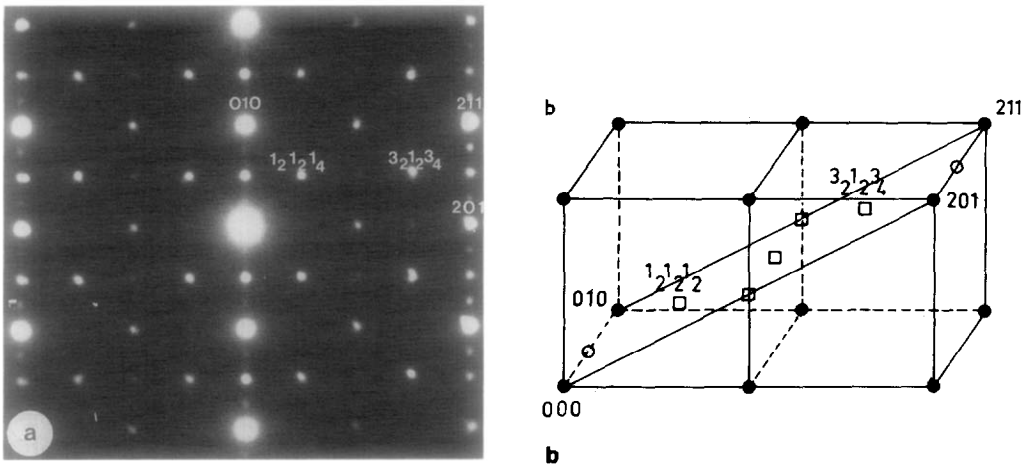

FIG. 3. (a) Electron diffraction pattern of the same crystal shown in Fig. 2a after tilting around b^* axis. Zone axis $[10\bar{2}]_c$. (b) Schematic representation of the above pattern within a reciprocal net corresponding to the pervoskite substructure.

diffraction and microscopy confirm that the nonstoichiometry is accommodated, as in LT samples, by means of disordered intergrowth of both B and G structures, as shown in Fig. 5. However, in these HT samples, the presence of the G phase is very small since the y values (see Table I) are 0.415 and 0.445 for $x = 0.7$ and $x = 0.8$, respectively, i.e., very close to the stoichiometric brownmillerite ($AMO_{2.5}$).

When $x = 0.9$, both X-ray and electron diffraction patterns correspond to the brownmillerite-type structure (a = 5.563(1) Å, b = 14.835(5) Å, c = 5.409(1) Å), the oxygen vacancies ($y = 0.475$), being, obviously, randomly distributed.

From the above results it can be seen that nonstoichiometry in HT samples of the Ca $Fe_xMn_{1-x}O_{3-y}$ system can be accommodated in several ways: microdomain formation ($0.2 \leq x \leq 0.6$), disordered intergrowths ($0.7 \leq x \leq 0.8$), and randomly dispersed oxygen deficiency ($x = 0.9$). The microdomains, which were not formed on LT samples, appear to be produced in a process of randomization of the superstructure among the three space directions. In fact, in the course of some oxido-reduction processes of these ferrites, three-dimensional microdomains are not only preserved

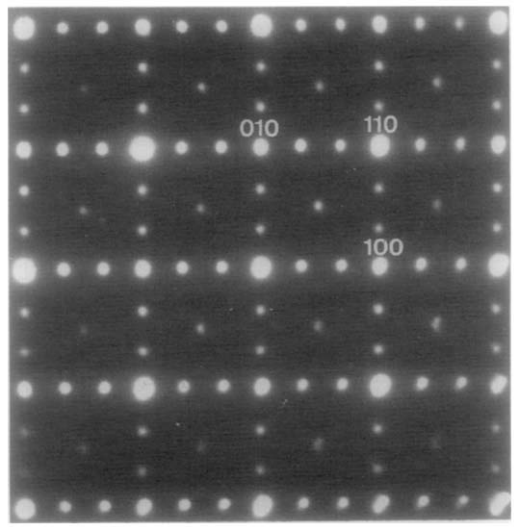

FIG. 4. Electron diffraction pattern of the second type of crystals found in the $x = 0.6$ material. Zone axis $[001]_c$.

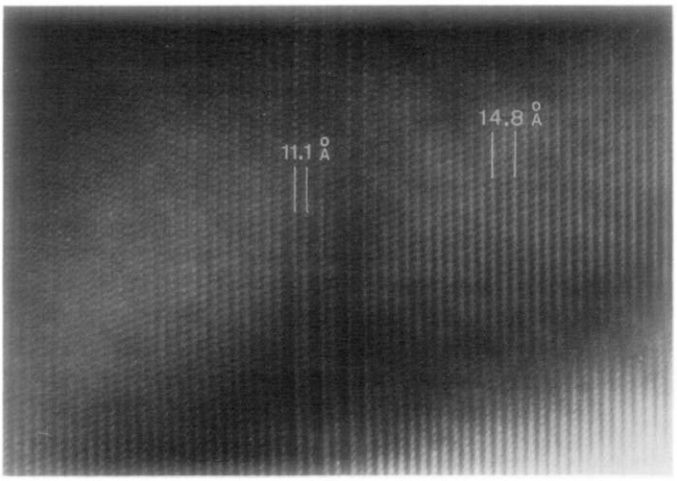

FIG. 5. Electron micrograph of the $x = 0.8$ sample along $[001]_c$.

but multiply and, depending on composition, structure, and thermodynamic conditions, three, six, or even nine sets of microdomains have been observed, by electron diffraction and microscopy, to coexist within one crystal (*2, 4, 13, 15*). It seems

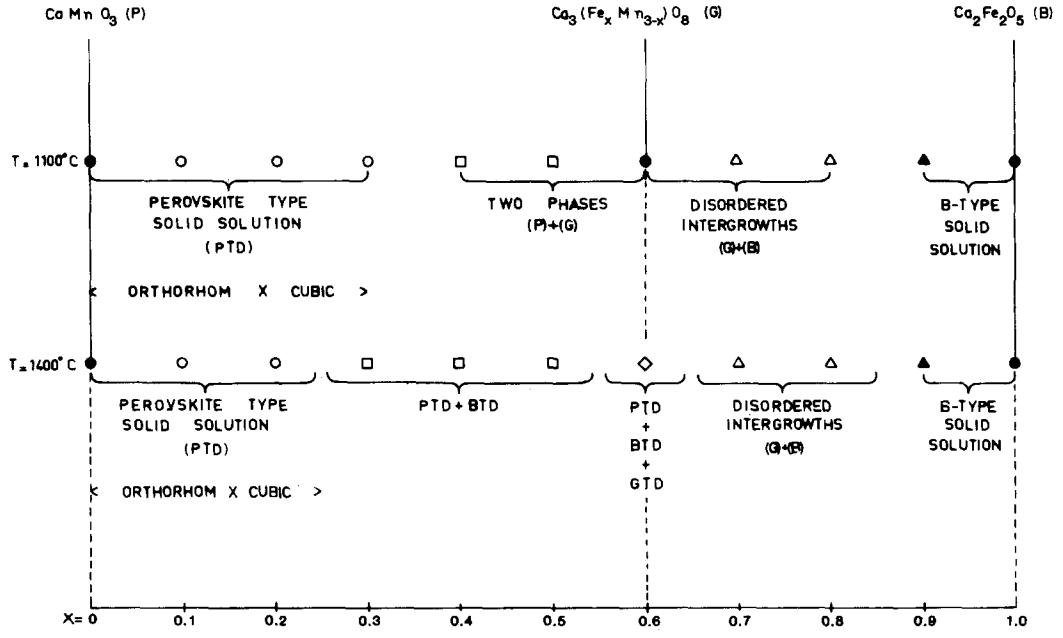

FIG. 6. Tentative phase diagram of the $CaFe_xMn_{1-x}O_{3-y}$ system as quenched from 1100 and 1400°C in air.

that the presence of two cations in different oxidation states occupying simultaneously either *A* or *M* positions of the perovskite substructure facilitates the oxidation process. We have already observed that undoped $Ca_2Fe_2O_5$ does not oxidize when heated up to 1400°C in air (*16*). Since chemical analysis data and Mössbauer spectroscopy studies (*17*) do not give evidence of Fe^{4+}, we must suppose that Mn^{4+} is entering $Ca_2Fe_2O_5$ to facilitate microdomain formation in the B structure. When the amount of Mn^{4+} is very small, no qualitative changes are observed between both HT and LT samples, compositional variations taking place by either isolated planar or point defects.

The study by electron diffraction and high-resolution electron microscopy of these materials confirms the important role that synthetic conditions play in the accommodation of nonstoichiometry. As a conclusion of the present work, a tentative phase diagram of the HT samples is presented in Fig. 6. It can be seen, by comparing with the LT samples, that the oxygen content is a function of the metal composition and annealing temperature, with in all cases, the HT phases being more reduced than the LT ones. The reason why microdomains are not formed in HT samples for $x \geq 0.7$ values seems to be, as discussed above, the tendency that $Ca_2Fe_2O_5$ shows to segregation, resulting in small areas richer in manganese where the oxygen excess is accommodated, originating slabs of the G phase which intergrowths in a disordered way with the B phase.

References

1. J. M. González-Calbet, J. Alonso, and M. Vallet-Regí, *J. Solid State Chem.* **71,** 331 (1987).
2. M. Vallet-Regí, J. M. González-Calbet, J. Verde, and M. A. Alario-Franco, *J. Solid State Chem.* **57,** 197 (1985).
3. J. Rodríguez, J. Fontcuberta, G. Longworth, M. Vallet-Regí, and J. M. González-Calbet, *J. Solid State Chem.* **73,** 57 (1988).
4. M. A. Alario-Franco, J. M. González-Calbet, and M. Vallet-Regí, *J. Solid State Chem.* **65,** 383 (1986).
5. H. D. Megaw, "Crystal Structures: A Working Approach," Sanders, London (1973).
6. E. F. Bertaut, L. Blum, and A. Sagnieres, *Acta Crystallogr.* **12,** 149 (1959).
7. J. C. Grenier, J. Darriet, M. Pouchard, and P. Hagenmuller, *Mater. Res. Bull.* **11,** 1219 (1976).
8. M. Hervieu, N. Nguyen, V. Caignaert, and B. Raveau, *Phys. Status Solidi A* **83,** 473 (1984).
9. W. S. Fyfe, *Nature (London)* **121,** 190 (1949).
10. W. S. Fyfe, *Anal. Chem.* **23,** 174 (1951).
11. R. D. Shannon and C. T. Prewitt, *Acta Crystallogr. Sect. B* **25,** 925 (1969).
12. M. A. Alario, M. J. R. Henche, M. Vallet, J. M. G. Calbet, J. C. Grenier, A. Wattiaux, and P. Hagenmuller, *J. Solid State Chem.* **46,** 23 (1983).
13. J. M. González-Calbet, M. Vallet-Regí, and M. A. Alario-Franco, *Inst. Phys. Conf. Ser.* **90,** 257 (1987).
14. J. C. Grenier, M. Pouchard, and P. Hagenmuller, *Structure Bonding* **47,** 1 (1981).
15. J. M. González-Calbet, M. Vallet-Regí, and M. A. Alario-Franco, *J. Solid State Chem.* **60,** 320 (1985).
16. M. A. Alario-Franco, J. M. González-Calbet, M. Vallet-Regí, and J. C. Grenier, *J. Solid State Chem.* **49,** 219 (1983).
17. J. Fontcuberta, J. Rodríguez, M. Vallet-Regí, J. Alonso, and J. M. González-Calbet, *J. Solid State Chem.*, in press.